AAS 01-154

Approaching Small Bodies

Anthony H. Taylor and John J. Bordi

Navigation and Mission Design Section
Jet Propulsion Laboratory
California Institute of Technology
4800 Oak Grove Drive
Pasadena, California 91109

This paper presents analysis of when and how well, on the approach to previously unvisited small bodies, the trajectory-design relevant physical parameters are determined. Quick acquisition of the knowledge of these parameters is required so that the orbital phase of a mission can be designed. We give the modeling assumptions and show covariance analysis results for a variety of conditions on the approach to four classes of small bodies ranging in diameter from 1 to 500 km. Time histories of the knowledge of mass, rotation characteristics, and comet outgassing are given for a variety of approach trajectories.

INTRODUCTION

This paper presents the results of analysis of the approach of a generic spacecraft to a variety of small bodies under the assumption that the parameters relevant to mission design are initially either poorly known or not known at all. The purpose of the analysis is to determine when and how well these parameters are determined so that an orbit phase can be designed to achieve mission scientific objectives. High velocity flybys are not a subject of this analysis.

All the solar system's planets except Pluto have been explored with orbital or flyby spacecraft, but only a few of its thousands of small bodies have been seen up close, and of these only one — Eros — has been orbited. The frontier of asteroids and comets is ripe for exploration, and there could be a multitude of orbital missions within the next few decades to the most reachable objects. Yet the very quality that makes these small bodies attractive for exploration — our ignorance of them — also presents the largest difficulty for designing and navigating missions about them. For most, the mass product, GM, is poorly known, yet reliable orbit design is reliant on precise knowledge of GM. For most, the rotation is either very poorly characterized or completely unknown and may be complex, involving off-principal-axis rotation, yet missions will require accurate rotational modeling to design orbits for efficient surface mapping or to target potential landing sites for high resolution close flybys. For comets, outgassing is a large unknown and presents an additional problem for design and navigation, since the forces on the spacecraft due to

outgassing may be larger than the gravitational forces. Thus, in contrast to traditional missions to the planets in which the orbit phase can be planned completely before launch, for most small body missions orbit design can only begin after arrival. Future missions need to understand when and how well the relevant parameters become known during the approach to previously unvisited bodies, and have some sense of "do"s and "don't"s for approaching these bodies.

The possibilities for mission, spacecraft, and small body parameters are conceptually illustrated in Figure 1 as a multidimensional scenario space where parameters take on values along the axes ranging from some minimum to maximum value. Our method is to generate scenarios to sample the space and use covariance analysis to evaluate the scenarios. This space is so large that there is no hope of sampling the volume to any reasonable density, and it must be pared down severely. We do this by evaluating a small number of reference cases, and then filling in the gaps where practical by taking variations on the reference scenarios. We hope that projects doing initial planning for small body missions will either be able to find a match with one of our scenarios or interpolate between them.

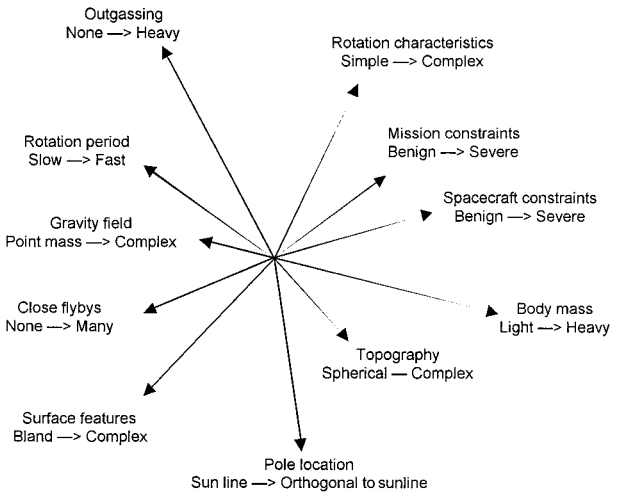

Figure 1 Multidimensional scenario space for orbit design and navigation at small bodies

HIGH LEVEL ASSUMPTIONS

We assume a generic mission to a comet or asteroid with the intent to orbit it at distances with periods on the order of 30 days or smaller. We address encounter geometries where the angle between the earth- and sun-lines at the body is relatively small, which in general would be the case for all encounters outside about 2 AU (where the maximum angle would be less than 30 degrees), although it would not exclude particular encounters inside that distance. The approach phase for the spacecraft (from now on called Generic for convenience) begins after the small body has been optically acquired by the onboard camera, Generic has been slowed to a velocity regime of meters per second (versus kilometers per second), and the small body camera image has grown large enough to designate landmarks and begin tracking them. We assume that during the high velocity heliocentric cruise phase Generic can be targeted to any desired

initial position within a few thousands of kilometers relative to the body and slowed so that the approach begins from that point.

Generic provides Doppler and ranging data to ground tracking stations, and the telecom parameters (frequency band, media calibrations, assumptions of oscillator stability and coherency, signal-to-noise ratio, etc.) are sufficient to always guarantee the accuracies given below in the detailed assumptions. Generic carries a camera whose accuracy also meets the detailed assumptions, and there are no constraints which would limit the camera pointing or optical data schedule such that the scenarios could not be flown. In practical terms, this probably means using an articulated camera, and probably articulated solar panels as well.

We use the orbit ephemeris for comet Temple 1 for convenience for all scenarios. During the time frame of all these scenarios, the body is in the post-perihelion phase of its orbit (Figure 2), at about 2.6 AU from the sun on 27 February 2006 at the beginning, and 2.8 AU on 31 March 2006 at the end. Since the time interval is short, the heliocentric orbit of the body approximates a straight line, the differential solar gravity is small, and therefore the spacecraft trajectory relative to the body is quite linear until it comes under the body's gravitational influence. This condition would apply to most missions except where the body is (e.g.) a planetary satellite in close orbit, or (e.g.) near perihelion of a highly eccentric heliocentric orbit.

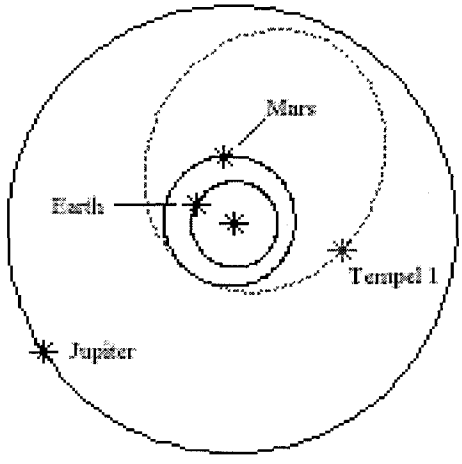

Figure 2 Heliocentric trajectory of the body at the beginning of approach (27 February 2006). Orbits of Earth, Mars, and Jupiter are shown for scale.

The body rotation may be complex (non-principal axis) or simple. It may have various levels of outgassing, from zero (asteroid) to "large" (comet) with a complex field. We assume the body has well-defined, uniformly distributed features which can be used as optical landmarks. Additionally, we assume that the comet outgassing and outdusting does not reduce the visibility of the landmarks or interfere with the camera imaging. Our analysis would not be applicable for approaching a body with a very bland surface without landmarks (e.g., deep layers of uniform dust).

DETAILED ASSUMPTIONS

Detailed physical and filter modeling is described here for the scenarios that we analyze.

Body size, mass and landmarks

Approaches are flown to the four bodies described in Table 1. Constant density ellipsoids are used for mass and gravity characteristics. The semi-axis ratios for Body 4 reflect the assumption that massive asteroids are more nearly spherical than the smaller bodies. Densities for bodies 1 and 2 are typical for comets, while the densities for 3 and 4 are more appropriate for asteroids. GM's and spherical harmonic gravity fields are computed and used to model the trajectories. However, we estimate only the GM term since there is little sensitivity to the harmonic coefficients over most of the trajectory and even at the end of the trajectory Generic is more that 30 radii from the body.

Table 1
BODY CHARACTERISTICS

Body	Largest Semi-axis (km)	Re* (km)	Ra† (km)	Density (gm/cm^3)	GM (km^3/s^2)	Description/ Examples (Re)
1	0.69	0.5	15.25	0.6	2.085e-8	Small comet Semi-axis ratios = 1 : .75 : .5 (X:Y:Z) Brooks 2 (.4), Wirtanen (.6), Churyumov-Gerasimenko (0.9)
2	4.16	3	100.7	0.8	6.004e-6	Moderate sized comet or small asteroid, Semi-axis ratios = 1 : .75 : .5 (X:Y:Z) du Toit-Hartley(2.2), Tempel 1 (3.1), Encke (3.7), Halley (5), Toutatis (2.3), McAuliffe (2.5)
3	34.63	25	1244	2.6	1.13e-2	Moderate sized asteroid or large comet, Semi-axis ratios = 1 : .75 : .5 (X:Y:Z) Eros (16.5), Ida (26), Mathilde (33), Schwassmann-Wachmann 1 (15), Hale-Bopp (25)
4	263.3	250	13040	3.0	13.03	Large asteroid Semi-axis ratios = 1 : .95 : .90 (X:Y:Z) Juno (120), Vesta (265), Pallas (285)

* Re = Radius of sphere with equal volume
† Ra = Radius at arrival = radius for a 30 day circular orbit

The nominal positions for optical landmarks for all 4 bodies are assumed at the spherical coordinate latitudes and longitudes shown in Table 2. Locations are chosen so that several (usually five or more) are in the line-of-sight from any viewpoint. Constraints are supplied to the initial landmark a priori uncertainties to, in effect, define a coordinate system. This is discussed in the subsection on the filter setup below.

Table 2
LANDMARK LOCATIONS

Landmark	Latitude (deg)	Longitude (deg)
1	0	0
2	0	60
3	0	120
4	0	180
5	0	–120
6	0	–60
7	45	30
8	45	150
9	45	–90
10	–45	90
11	–45	–150
12	–45	–30
13	80	90
14	–80	–90

Figure 3 shows the ellipsoidal shape for any of the first three bodies. A landmark is treated by the filter as visible in an optical frame only if it is on the day side of the body terminator as well as in the line-of-sight. A few hundred landmarks might be used on an actual mission (e.g. NEAR), but for this covariance analysis fourteen are adequate.

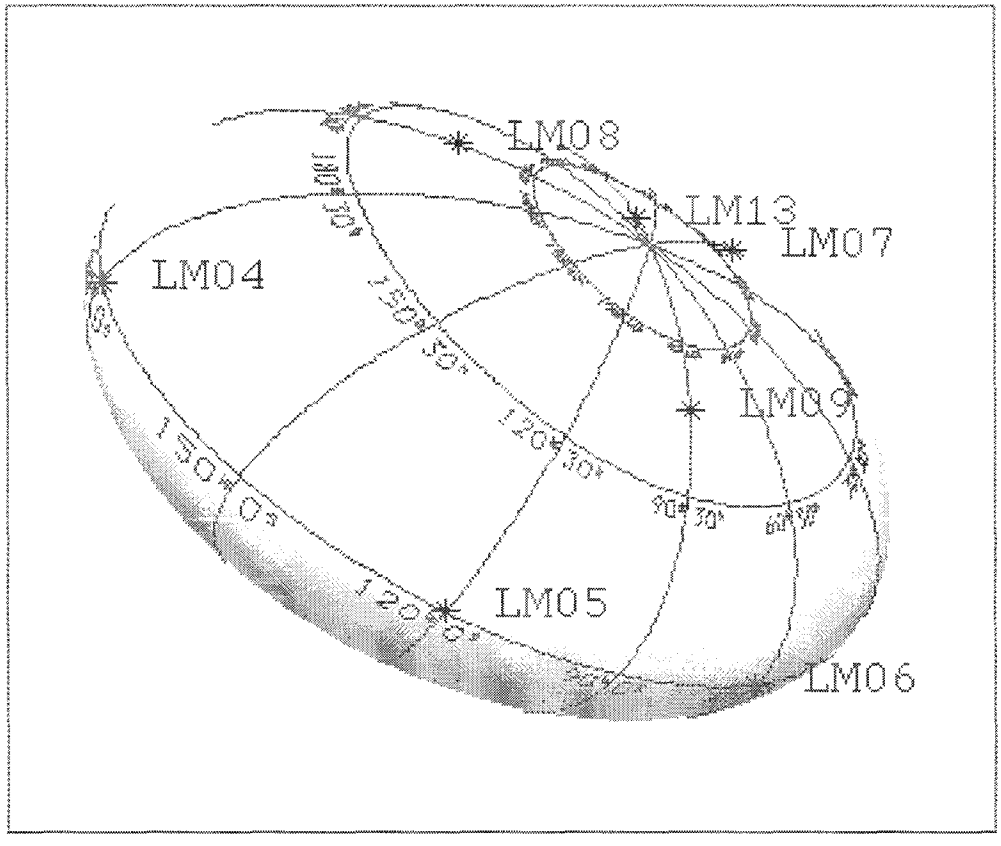

Figure 3 Ellipsoid used for Bodies 1–3, with 7 landmarks in the line-of-sight

Trajectory coordinate system

Trajectories in the following sections are described by angles in a sun oriented clock/cone system centered on the small body. The Z-axis points to the sun, and the cone angle of a point (e.g., the spacecraft) is the angle of the point from this axis. The clock angle is measured in the X-Y plane positive from X toward Y, where X and Y are perpendicular to Z and Y is in the direction of the cross product of the Z-axis with the ecliptic north pole (i.e., if the body is in the plane of the ecliptic, Y is also in the plane of the ecliptic and X is along the ecliptic pole).

Approach trajectories

While mission designers have no control over the physical parameters associated with a comet or asteroid, they do have the latitude to design approach trajectories to minimize hazards and mission costs while maximizing the rate of knowledge return. We have chosen to sample this part of scenario space as simply as possible with a few (nearly) straight-line trajectories. Each trajectory begins when the body image has grown to a diameter of a few tens of camera pixels (~33 for Body 2) and landmarks can first be designated and tracked, and ends at a radius at which a 30 day circular orbit could be entered. The beginning approximately marks the earliest time that optical data about rotation and shape can begin

accumulating. The arrival marks the place where the initial orbital phase might begin, not so far out as to have an unacceptably long orbital period, and not so close in as to constitute a hazard in an unknown environment.

Time is an important mission parameter, since tracking schedules must be negotiated well in advance of arrival, and command loads for observations, maneuvers and other operations must be designed, uplinked and executed accordingly. Short approach times drive up risks because of the unknown environment, particularly for active comets, while long ones drive up costs. We balance those factors by choosing about a month — 32 days — for the approach time of the reference scenarios. The times, distances, and velocities are given in Table 3, where a slowing maneuver is assumed 11 days before arrival and a circularizing maneuver may be executed upon arrival. Approach directions will be discussed momentarily.

Body 2 was used as a benchmark for sizing reasonable approach times, distances, and velocities in Table 3. Distances in the table were then scaled for the other bodies by $d_i = (\rho_i/\rho_2)^{\frac{1}{3}}(R_i/R_2)d_2$, and the velocities were adjusted to keep the approach times constant. Scaling trajectories by the above relation, where ρ is the density and R is the body spherical effective radius, yields constant circular orbit periods if distance d is an orbit radius, and this results in equivalent end points for all the bodies (i.e., the radius for a 30 day orbit period). If the densities were the same for all the bodies, then the beginning points defined by the diameter of the optical image would also be equivalent, but since they are not, we accept some variation in the definition of the beginning point for the sake of simplicity. The image angular diameter at the initial point ranges from 23 pixels for body 4 to 39 pixels for body 1.

All of the approach velocities are tenable for hydrazine-fueled spacecraft, and for the smallest 3 bodies they are tenable for SEP powered spacecraft, but for a Vesta class approach with SEP thrusting, a longer approach time with lower velocities would be required.

Table 3
APPROACH TIMES, RADII, AND SPEEDS

	Body 1		Body 2		Body 3		Body 4	
Days before arrival	**R (km)**	**V(km/s)**	**R (km)**	**V(km/s)**	**R (km)**	**V(km/s)**	**R (km)**	**V(km/s)**
32	1500	~0.74	10000	~5 m/s	123500	~61	1295000	~642
11	150	~0.14	1000	~1 m/s	12350	~12	129500	~123
0	15.3	0.04*	101	0.24*	1244	3.0*	13040	31.6*

* Circular orbit velocity for 30 day period

Direction of approach is one of our variables in scenario space. We assume that the heliocentric cruise trajectory can be designed to place Generic at any desired location relative to the body at the beginning of the approach phase and that the spacecraft can be left with the velocity given in Table 3 directly toward the body at that time. This is certainly a reasonable assumption for bodies 1 and 2, given the short distances involved, and probably 3 and 4 as well. Now two questions arise: (1) Where should the initial approach point be, or equivalently, what is the best direction of approach to the body? and (2) Where should the trajectory be targeted to intercept the radius of the 30 day circular orbit? The scenarios described in Table 4 and illustrated in Figure 4 were designed to address those questions.

There are several competing factors involved in selecting the approach direction:
Optical data: More of the illuminated portion of the body is visible for trajectories near 0° solar phase angle, which means that there are more landmark observations available to determine parameters. From

this consideration, the 0° approach is best and the 135° approach is worst. (We ignore possible effects like poor relief and wash-out of features which might actually make the 0° trajectory undesirable). We do not consider a 180° approach, since *no* landmark data is available.

Radiometric data: Since we assume encounter geometries in which the angle between the earth-line and sun-line is small (e.g., encounter > 2 AU), approaching along the sun-line is nearly equivalent to approaching along the earth-line, along which the Doppler data is most sensitive for determination of mass. The worst direction for radiometric sensitivity would be the 90° trajectory, while the 135° trajectory would result in an intermediate sensitivity.

Comet outgassing: Since outgassing is a strong function of solar phase angle, peaking near 0°, and since forces from outgassing can be as large or larger than the body gravity forces, approaching along the sun line may be the worst scenario for early determination of body mass. Additionally, the solar panels will be face-on to the dynamic pressure direction. Approaching in the plane of the terminator, Generic experiences much less dynamic pressure (typically by a factor of 10), and the solar panels present a minimum aspect. Unfortunately this is also when Doppler sensitivity to mass is smallest, and this fact leads us to consider the 135° trajectory on which there is even lower dynamic pressure and at least moderate Doppler sensitivity.

Table 4
SCENARIOS FOR APPROACH DIRECTION AND ARRIVAL POINT

Case	Approach Direction	Arrival Point
1	Along 0° cone angle (sun-line)	In the terminator plane (cone = 90°) at tangent point to sphere of radius Ra, at clock = 0° (on X-axis).
2	Toward body along 90° cone angle (in terminator plane)	Same as Case 1
3	Toward body along 135° cone angle (on dark side of terminator plane)	Same as Case 1
4	Toward body along 0° cone angle (sun-line)	At 0° cone angle where it intercepts sphere of radius Ra
5	Toward body along 90° cone angle (in terminator plane)	At 0° phase angle at tangent point to sphere of radius Ra
6	Toward body along 135° cone angle	At 45° phase angle at tangent point to sphere of radius Ra

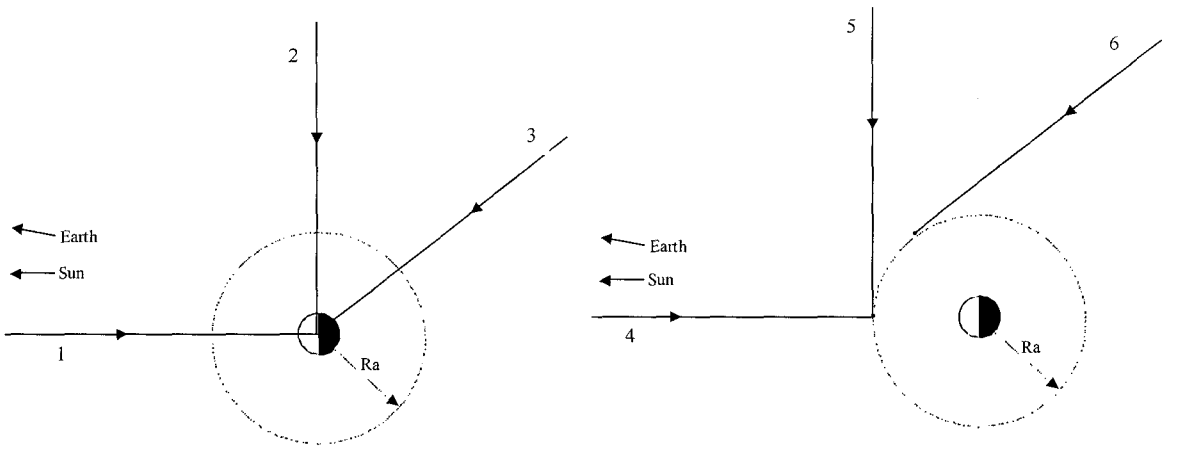

Figure 4 Cartoon showing the 6 trajectories described in Table 4. Trajectories 1, 2 and 3 end at a common point above the body terminator at a radius of Ra. Trajectories 4 and 5 end at a common point on the body-sun-line at a radius of Ra, and trajectory 6 ends where it becomes tangent to a sphere of radius Ra.

The arrival points were selected to mitigate some of the undesirable features of the approach directions discussed above. For example, trajectory 1 ends in the terminator plane where Doppler sensitivity to the body mass is nominally zero, while trajectory 4 allows an initial orbit to be entered at a point where mass knowledge might be improved, depending on the severity of outgassing. Endpoints of trajectories 2 versus 5 and 3 versus 6 were selected for the same rationale.

Comet Outgassing

The outgassing drag pressure model uses the formulation of Scheeres (Ref 8) in which modified spherical harmonics determine the magnitude of the drag pressure field,

$$P_a(r,\phi,\lambda)=\frac{P_d}{r^2}\left[1+\sum_{i=1}^{N}\sum_{j=0}^{i}P_{ij}(\cos\phi)\{\alpha_{ij}\cos(j\lambda)+\beta_{ij}\sin(j\lambda)\}\right]$$

where the units of P_a are Nt/m^2, the P_{ij} are the associated Legendre functions, α_{ij} and β_{ij} are unitless, and P_d has units of $Nt\cdot km^2/m^2$ when r, the range of the spacecraft from the body center, is in *km*. ϕ is the cone angle described earlier, while λ is a clock angle relative to an X-axis that is in the plane defined by the Z-axis (sun-line) and the velocity vector of the body. (This is different from the X-axis defined earlier for trajectory definitions, but the distinction is unimportant for the purpose of this analysis, since the outgassing field is close to symmetric about the Z-axis.) The values of P_d, α_{ij} and β_{ij} up to $i=4, j=4$, were supplied by Scheeres et al. by fitting to a numerically computed outgassing field supplied by Enzian, et al. (Ref 1) for comet Tempel 1 at 2 AU. Enzian's numerical pressure field acted primarily in the radial direction, and the harmonic representation used here assumes the field is purely radial. The field is static in the sense that it is not modulated by the rotation of the comet, but we do apply stochastic variations as described in the subsection on the filter setup. The acceleration due to the field is

$$\ddot{\mathbf{R}}=\frac{kP_dA}{M}\hat{\mathbf{r}}$$

where $\hat{\mathbf{r}}$ is a unit vector in the radial direction, M is spacecraft mass, A is the total projected area in the radial direction, and k is a scale constant which we use to adjust the overall magnitude of the field. We model Generic's surface as a large solar panel typical of a SEP spacecraft, $A_p = 100\,m^2$, which is always sun pointed plus a spherical bus of cross-sectional area $A_b = \pi\,m^2$. Then, the projected area $A = (A_p \cos(\phi) + A_b)$. P_d, which gives the overall strength of the field, is provided by Scheeres for Tempel 1 at 2 AU. In actuality we adjust k to yield the magnitude of acceleration that we want for different outgassing scenarios while keeping the shape of the field the same. That shape is defined by the α_{ij} and β_{ij} values in the Appendix.

Figure 5 shows a contour plot of the shape and magnitude of the acceleration field as we scale it for Body2. Acceleration was adjusted to be equal and opposite to the gravitational acceleration along the 0 degree solar phase angle. Estimates of outgassing by different experts vary by an order of magnitude or more, and this level of acceleration is a reasonable possibility, especially for the larger solar arrays associated with SEP spacecraft. From Figure 5 it is easy to see that determination of body mass may be easier when approaching at or behind the body terminator plane.

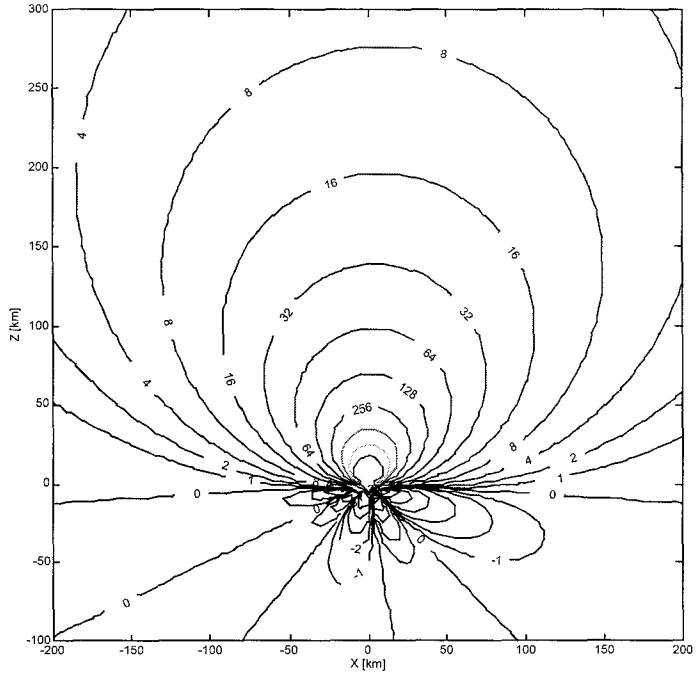

Figure 5 Radial acceleration due to gas pressure, Body2 [nano-g]

The pressure fields for Bodies 1 and 3 were scaled by the ratio of their surface areas to that of Body 2. Since the outgassing acceleration varies with the square of the body radius while gravity varies with the cube, the outgassing forces dominate on the sunward side of the comet for Body 1. On the other hand, the gravitational forces predominate over the outgassing forces everywhere for Body 3.

Body rotation characteristics

Very little is known about the rotation characteristics of most small bodies, including the mode of rotation or direction of the pole. Although it is expected that most asteroids will be in principal axis rotation, there are exceptions of which Toutatis is an example. Active comets are more likely than asteroids to be in non-principal axis rotation due to outgassing. For missions to any unvisited small bodies, projects must be prepared to model and estimate general rotations, from simple to complex. Additionally, they should have the capability to quickly plan (or replan) an orbit phase to accommodate a science observation campaign to the rotation that is found.

We model and estimate the three rotation scenarios given in Table 5, and the directions of the angular momentum poles in Table 6. The ratios of principal axes that we use for bodies 1, 2 and 3 correspond to ratios of principal moments of inertia of (Ix : Iy : Iz) = (0.521 : 0.799 : 1), and the ratios for body 4 are (0.900 : 0.951 : 1).

Table 5
SCENARIOS FOR ROTATION MODES

Case	Characterization	Principal axis ratios X:Y:Z	Spin at arrival			RMI*
			Lon (deg)	Lat (deg)	Rate (deg/s)	
1	Principal axis rotation about Z	Any	N/A	90	.012500	1.00
2	Non-principal axis rotation. SAM rotation	1 : .75 : .50	0	45	.013106	0.19
3	Non-principal axis rotation. SAM rotation	1 : .95 : .90	0	70	.012507	0.78

* Rotation Mode Index

Table 6
SCENARIOS FOR POLE ORIENTATION

Case	Direction of angular momentum pole at arrival
1	Sun pointed
2	45° from sun-line, 0° clock angle from ecliptic pole.
3	45° from sun-line, –45° clock angle from ecliptic pole.
4	90° from sun-line, 0° clock angle from ecliptic pole.

The RMI parameter in Table 5 is a measure of rotation complexity. For its definition, we adopt the nomenclature of Scheeres (Ref 7) for the effective rotation rate, ω_I, and dynamic inertia, I_D, for a given body

$$\omega_I = \frac{\Omega \cdot \mathbf{I} \cdot \Omega}{|\mathbf{I} \cdot \Omega|} \; ; \; I_D = \frac{\Omega \cdot \mathbf{I} \cdot \mathbf{I} \cdot \Omega}{\Omega \cdot \mathbf{I} \cdot \Omega}$$

This is the equivalent rotation rate and moment of inertia of a rotating sphere with the same angular momentum and kinetic energy. For all the cases in Table 5, we use an effective rotation rate of 0.0125 degrees/second which yields an effective period of 8 hours. The size of I_D relative to the principal moments of inertia determines the modes of rotation of a body. Defining the "Rotation Mode Index":

$$RMI \begin{cases} = (I_D - I_y)/(I_z - I_y); & I_D \geq I_y \\ = (I_D - I_y)/(I_y - I_x); & I_D < I_y \end{cases}$$

when RMI > 0 the body is in SAM (Short Axis Mode) rotation in which the body precesses about the Z axis (except when RMI = 1, when there is simple rotation about Z). RMI < 0 signifies LAM (Long Axis

Mode) rotation in which the body precesses about the X axis (except when RMI = -1, when there is simple rotation about X). (Ref 7). For RMI close to + or – 1, the rotation is relatively simple, while for values approaching 0, the rotation becomes more complex, and the angular velocity vector begins swapping directions between the +Y and – Y axes. The rotation for Case 2 of Table 5 is moderately complex, with the angle of the Z axis varying between 28 and 62° from the angular momentum pole. For Case 3, the angle varies between 18 and 28°.

Figure 6 shows that landmark tracking may be considerably improved for complex rotation.

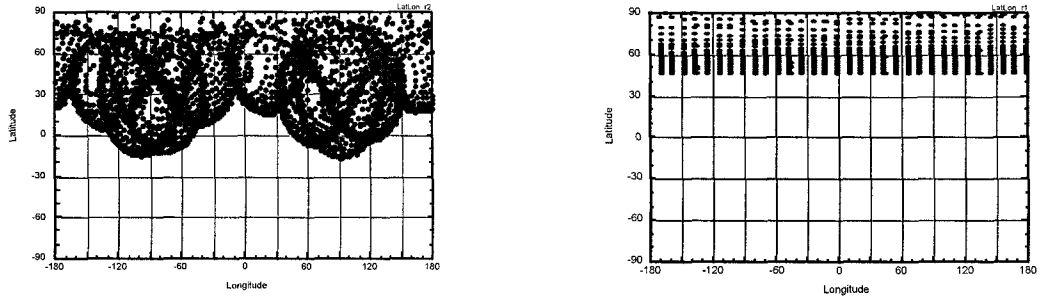

Figure 6 Latitude vs. Longitude of the sub-spacecraft point at 15 minute intervals for Rotation Mode Case 2 (complex rotation) on the left, and Case 1 (simple rotation) on the right. Much more of the body surface is seen by the spacecraft for the complex case. (Pole Orientation Case 2 is used for both plots.)

Spacecraft parameters

The properties of Generic relevant to this analysis are given in Table 7. The solar panel size is typical for a spacecraft using Solar Electric Propulsion (SEP), which makes it more susceptible to the effects of outgassing than spacecraft using chemical propulsion. We use surface reflectivity properties typical of most spacecraft, which result in the acceleration due to solar pressure as given in the table. We assume there are no constraints on camera pointing and that the solar panels are always oriented to the sun. The given pixel resolution would be expected of (e.g.) a camera with a 1 degree diameter field of view using a 1024 x 1024 square pixel array. In terms of dynamic noise, Generic is a moderately quiet spacecraft, e.g., 3-axis stabilized with coupled thrusters.

Table 7
SPACECRAFT CHARACTERISTICS

670 kg	Mass
100 m^2	Solar array area (always sun pointed)
3.1 m^2	Bus area (cross-section of a 1 m radius sphere)
17e-6 rad/px	Camera pixel resolution
16 nano-g	Solar pressure acceleration due to solar panels + bus at -11 days

Mission parameters

Missions prefer to minimize data quantities because of high costs for sequence building, tracking, and ground processing. Since there is a trade-off between cost and getting sufficient data to do the job, we analyze scenarios for which there is more or less data available, as in Table 8. The average DSN pass

length is about 8 hours.

Table 8
SCENARIOS FOR DATA SCHEDULES

Data Case	Description
1	All available DSN passes for radiometric tracking (3 per day), 1 optical navigation frame every 3 hours.
2	Every other available DSN radiometric pass, 1 optical navigation pass every 6 hours.
3	1 DSN radiometric pass per day, 1 optical navigation frame every 12 hours.
4	Radiometric data only, every other available DSN pass.
5	Optical navigation data only, 1 frame every 6 hours.

Filter setup

The filter parameter and data accuracy assumptions are given in Tables 9 and 10. A total of 120 parameters are estimated, 7 of them stochastically. The 9 tracking station coordinates are not estimated but the effect of their errors are included in the results. Large a priori uncertainties are assumed for the main parameters of interest at the small body: mass and inertia tensor, rotation, outgassing, and landmark locations. Most of the rest of the uncertainties are representative of current modeling capabilities.

A coordinate system for any new body will likely be defined relative to landmarks on its surface by assigning coordinate values to selected landmark locations. Six quantities need to be fixed: three for the location of the origin and three for the orientation of the axes. We accomplish this in the filter by assuming a priori errors of zero for the latitudes and longitudes of three widely separated landmarks, thus constraining those coordinates to their nominal values in Table 2.

The optical landmark accuracies of Table 10 are representative of the accuracies found on the NEAR mission (Ref 6). The change from the 3 pixel to 1 pixel uncertainties in the optical landmark observations corresponds to when the apparent diameter of Body 2 reaches approximately 70 pixels.

Table 9
FILTER PARAMETERS

Parameters	A Priori Uncertainty (1-σ)	Comments
Estimated as bias:		
Epoch state (6)	1e6 km, 1 km/s per axis	
Cartesian acceleration (3)	0.1 nano-g	Attitude thruster mismodeling
Maneuvers (3)	0.1*ΔV per axis	11 days before arrival, xyz components
Solar pressure effective area (2)	5% of nominal area	Solar panels and spherical body
Drag coefficient (1)	5% of nominal drag coefficient	Due to outgassing
Body epoch attitude (3)	Infinity per axis	RA, Dec of Z axis, prime meridian angle.
Body epoch spin vector (3)	0.05°/s	~4*nominal spin vector magnitude
Body GM (1)	100% of nominal GM	For GM of each body
Body inertia tensor (6)	~2*max nominal moment of inertia.	For each of the 6 independent elements
Outgassing scaling parameter (1)	200% of nominal	
Outgassing harmonic coefficients (30)	200% of nominal α(i,j) coefficients for α(i,j) and β(i,j)	
Landmarks (42)	Longitude: 360° Latitude: 180° 200% of Re of body	Latitude and Longitude of landmarks 1, 3 & 7 constrained by setting sigmas = 0.
Body heliocentric ephemeris (6)	Covariance (~300 km)	Tempel 1 covariance (Ref 16)
Earth heliocentric ephemeris (6)	Covariance DE405	(Ref 13)
Estimated as stochastic:		
Earth polar motion (2)	30 cm per axis	τ = 2 days
Earth timing (UT1) (1)	45 cm	τ = 1 day
Outgassing scaling parameter (1)	50% of nominal	τ = 8 hours
Cartesian acceleration (3)	0.02 nano-g	τ = 8 hours. Attitude thruster mismodeling
Considered:		
Tracking station locations (9)	15 cm per axis	Sufficiently conservative to cover media errors as well.

Table 10
DATA ACCURACIES

Data Type	Gaussian noise (1-σ)	Comments
DSN Doppler	0.2 mm/s per 1 minute measurement	Typical for X-band coherent tracking.
DSN ranging	5 m	1 measurement per pass
Optical landmarks	Before Arrival – 20d: 3 pixels After Arrival – 20d: 1 pixel	Assumes pointing knowledge gained from

		stars in same frame.

RESULTS

In this section, the first subsections present the results for four reference cases, one for each category of body, while the later subsections explore variations to the reference cases to see their impact on the estimated parameters. Wherever uncertainties are discussed in this section, they are always 1-sigma values. The conditions for the reference cases are shown in Table 11. Since outgassing is turned on for the first three bodies, they are actually comets while the fourth is an asteroid.

Table 11
REFERENCE CASES

Assumption	Body 1	Body 2	Body 3	Body 4
Trajectory (see Table 4)	Along Sun-line (Case #1)	Along Sun-line (Case #1)	Along Sun-line (Case #1)	Along Sun-line (Case #1)
Pole Orientation (see Table 6)	45° cone, 0° clock (Case #2)	45° cone, 0° clock (Case #2)	45° cone, 0° clock (Case #2)	45° cone, 0° clock (Case #2)
Rotation (see Table 5)	Complex (Case #2)	Complex (Case #2)	Complex (Case #2)	Simple (Case #1)
Outgassing	Yes	Yes	Yes	No
Tracking Data Rates (Table 8)	Medium rate (Case #2)	Medium rate (Case #2)	Medium rate (Case #2)	Medium rate (Case #2)

Reference Cases – Mass and Outgassing

Body mass should be determined as early in the approach as possible so that detailed orbit planning can begin and reach completion before arrival. Figure 7 shows the uncertainty in the estimated GM versus time before arrival for each reference case, where the a priori uncertainty was assumed to be 100% of the nominal mass for each body. As indicated, the mass of each of the two lighter bodies is very poorly determined, while for the massive bodies it is well determined early-on. This is explained by two considerations:

(1) As a result of our scaling of the trajectories, the ratio of spacecraft gravitational accelerations at equivalent epochs for bodies i and j is $a_i/a_j = (R_i/R_j)(\rho_i/\rho_j)^{1/3}$. For example, the ratio for bodies 3 and 2 is $a_3/a_2 = 12.3$. In the presence of dynamic and data noise, this corresponds to a stronger signal to noise ratio, which allows quicker determination of the larger mass.

(2) Outgassing is more a factor for smaller bodies than larger ones in general because (all other considerations being equal) outgassing forces should scale with the square of body radius while mass scales with the cube. This is the way they are scaled for our reference cases, and the resulting relative strengths between outgassing and gravitation forces can be seen by superimposing them as in Figures 8–10.

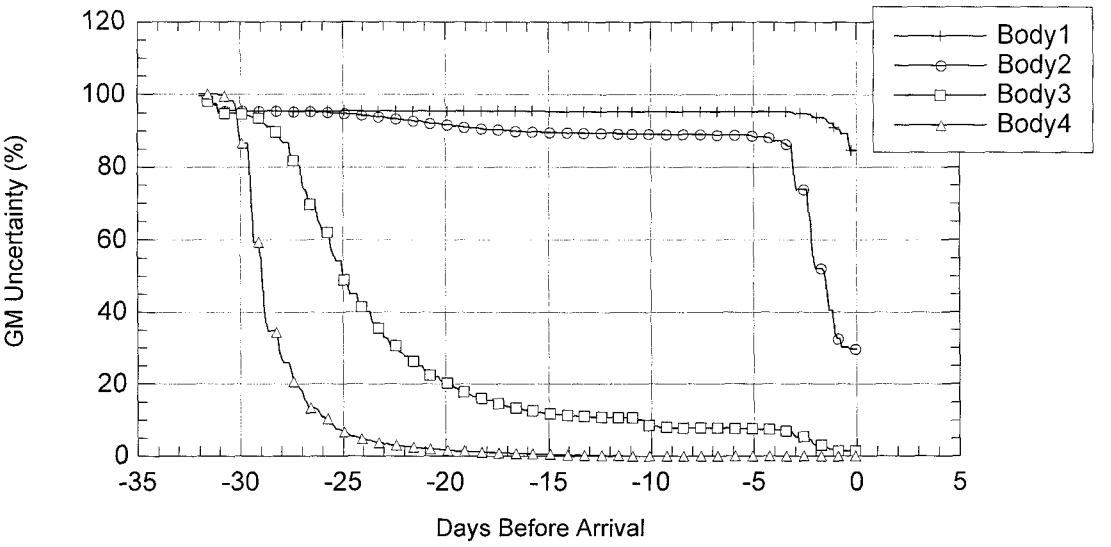

Figure 7 GM 1-σ uncertainty as a percentage of nominal for the four reference cases

From Figures 8 and 9 it is easy to understand the poor performance at Bodies 1 and 2, since the spacecraft approaches along the sun-line (Z-axis) where outgassing / gravity acceleration is large. Both mass estimates improve at the end as the spacecraft enters the region near the terminator plane where gravity dominates. Figure 10 shows that gravitational forces predominate everywhere for Body 3, and thus the mass is estimated quickly. Body 4, of course, has no outgassing.

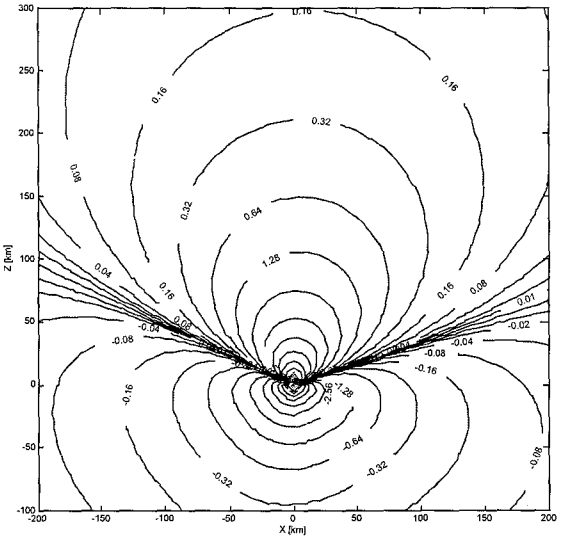

Figure 8 Superimposed gas and gravitational accelerations near Body 1 [nano-g]

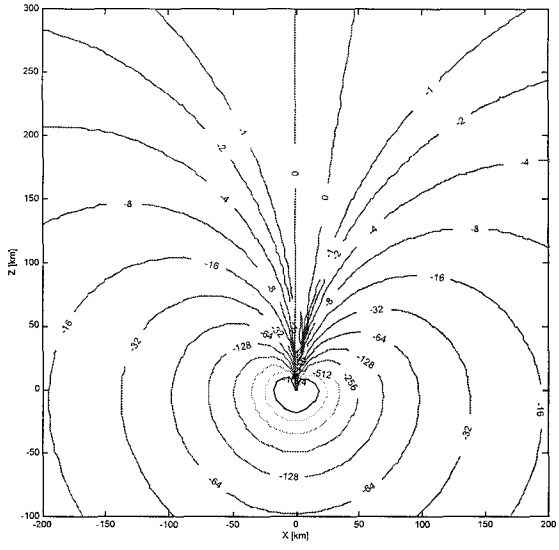

Figure 9 Superimposed gas and gravitational accelerations near Body 2 [nano-g]

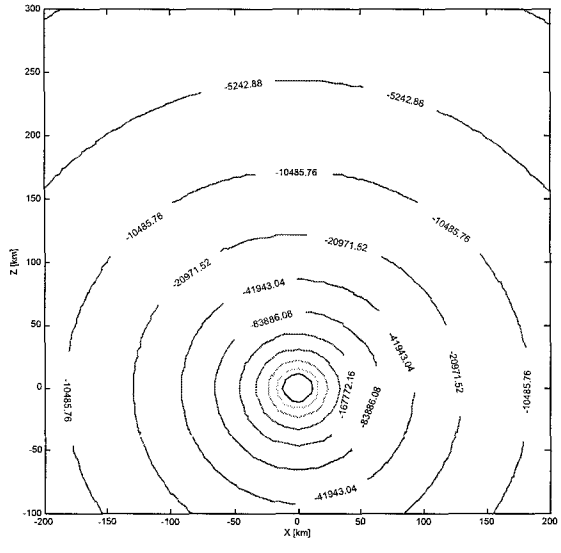

Figure 10 Superimposed gas and gravitational accelerations near Body 3 [nano-g]

Given the above figures, it is easy to understand some of the features of Figure 11 where the estimate of the bias component of the outgassing strength factor, P_d versus time, is shown. The outgassing strength is determined most quickly for the smallest body and last for the largest. The downward step in the uncertainty at –11 days in the Body 3 case corresponds to the slowing of the approach speed that coincides with the slow down maneuver. We have not yet come to a conclusion as to why this should occur, nor do we understand yet why there seems to be a floor near 58% for all three outgassing cases, but we suspect that the latter effect is due to a combination of the effects of the dynamic noise introduced by the stochastic component of P_d, and aliasing between the bias P_d and the 30 poorly determined harmonic coefficients of the outgassing model.

It should be noted that orientation of the solar panels may have a large effect on determination of both outgassing and mass (particularly in the later phase of the approach when gas drag would dominate over solar pressure force) and we have not addressed that here. Determination of both outgassing and mass could well be significantly improved by changing the aspect of the solar panels periodically relative to the outgassing flow and observing the changes in acceleration in the Doppler tracking data or the changes in torque on the spacecraft by monitoring the effect on reaction wheels or attitude thruster activity.

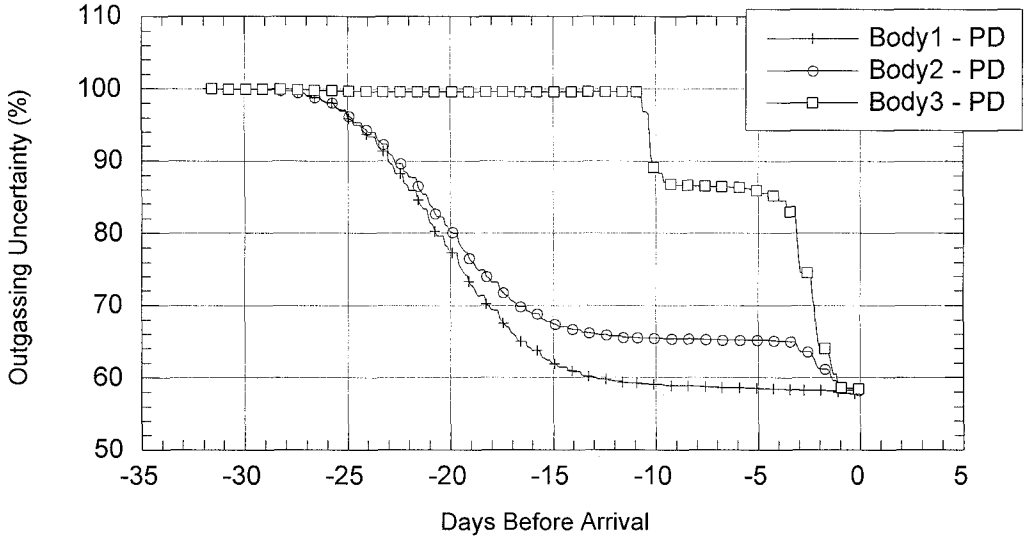

Figure 11 Outgassing strength 1-σ uncertainty for the three comet reference cases

For mission planning, the mass estimates for Bodies 3 and 4 are probably good enough by –15 days or earlier for detailed orbit planning to begin, assuming that other parameters have also been sufficiently well determined. For Bodies 1 and 2, mass is not well enough known for detailed planning unless the mission has decided a priori that it will forego ballistic trajectories and power the spacecraft around the bodies using thrusters, at considerable expense of fuel. For these smaller bodies it may be desirable to approach along a trajectory near the plane of the terminator or behind it, which we address in the "Variations – Approach Trajectories" subsection.

Reference Cases – Body Attitude

Early knowledge of the rotation characteristics (direction of angular momentum vector, effective period, ratio of principal axes of inertia, and rotation mode index) is important for designing orbits to achieve maximum instrument coverage, particularly for imaging instruments so that as much of the surface as possible can be mapped in a minimal time. For example, orbit orientations would likely be designed completely differently for a pole (1) pointed at the sun, (2) orthogonal to the sun line, or (3) intermediate between sun-pointed and sun-orthogonal. The rotation period and complexity will also strongly affect decisions about the orbital period, shape, and orientation.

Since the rotation characteristics are not directly estimated, their uncertainties must be derived from the covariances of the estimated parameters. We have only recently begun those derivations and our analysis is yet too young to present here, so we talk instead to body attitude (which is also derived and in which we have more confidence) under the reasonable assumption that knowledge and predictability of attitude versus time is equivalent to knowledge of the rotation characteristics. We specify attitude knowledge in the following figures and tables by determining the uncertainties for the right ascension and declination of the body-fixed Z-axis and the uncertainty of the orientation angle of the X-axis about Z, all

relative to the Earth Mean Orbit and IAU vector of J2000 coordinate frame, and then RSSing these three uncertainties into one quantity which we call the attitude uncertainty.

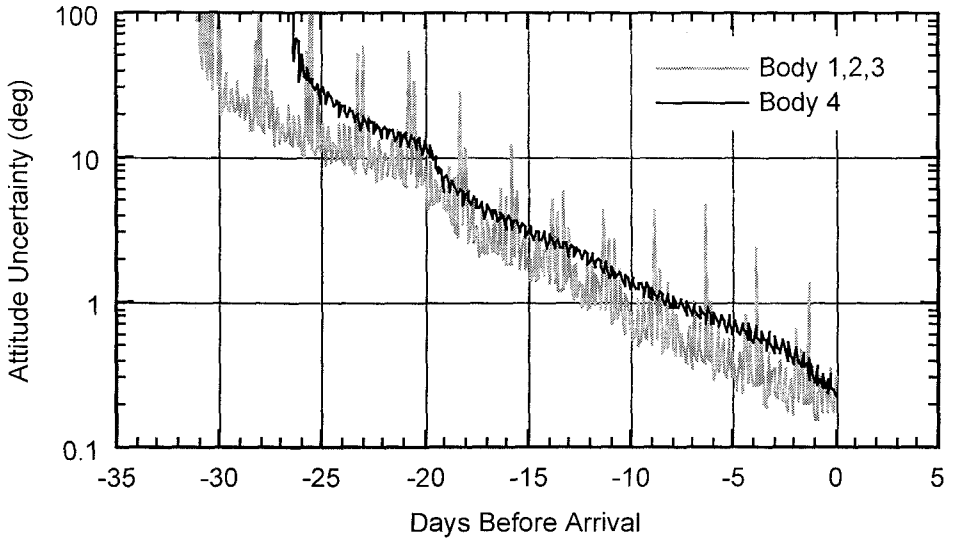

Figure 12 Attitude 1-σ uncertainties for Body 1–4 reference cases. RSS of three angles (Z-axis right ascension and declination and X-axis rotation). To reduce clutter, only Body 2 is plotted for the data labeled "Body 1,2,3", but it is representative of all three bodies.

Figure 12 shows the attitude knowledge time history for all four bodies. (The history for Bodies 1–3 are so similar that only one of is plotted to reduce clutter.) The knowledge for Body 4 has a similar history but is slightly worse on average, although the curve does not exhibit the spikes seen in the other three bodies. These effects are due to the simple (Z-axis rotation) of Body 4 versus the complex rotation of the other three (which is identical for all three). The spikes in the uncertainties of the complex rotators is artificial, due to inflation of the right ascension uncertainties when the Z-axis wanders near the pole of the inertial system (we did not adjusted it by the cosine of the declination before RSSing). The slightly worse results of Body 4 are probably due to the reduced set of landmarks available to be imaged as the spacecraft approaches. In Figure 13, which compares time histories of observability for the 14 landmarks, four landmarks are never seen on the approach to Body 4 because they are on the hemisphere tilted away from the spacecraft, whereas all landmarks are available on the other three bodies because of the "turbulence" of their rotation. The slight improvement for all bodies just after –20 days occurs because of the application of tighter weighting on the optical data at that time.

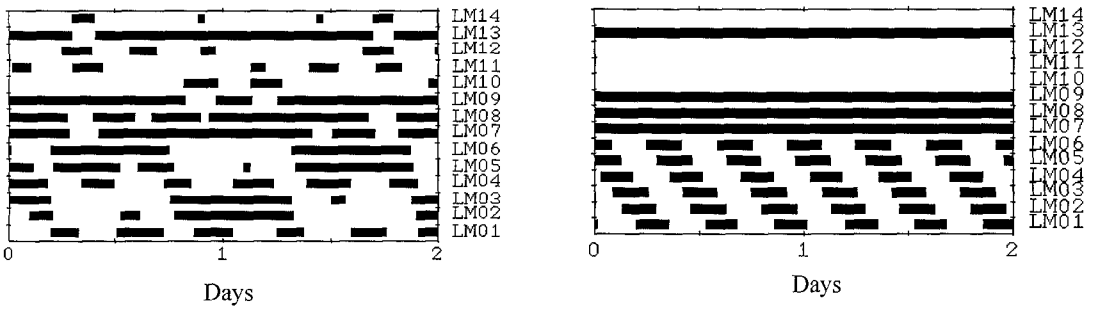

Figure 13 Observability of landmarks during the approach for complex rotation on the left (Body

1–3 reference cases) and simple rotation (Body 4) on the right. Landmarks are observable when they are both illuminated by the sun and line-of-sight visible to the spacecraft. Two days are shown, near the beginning of the trajectory.

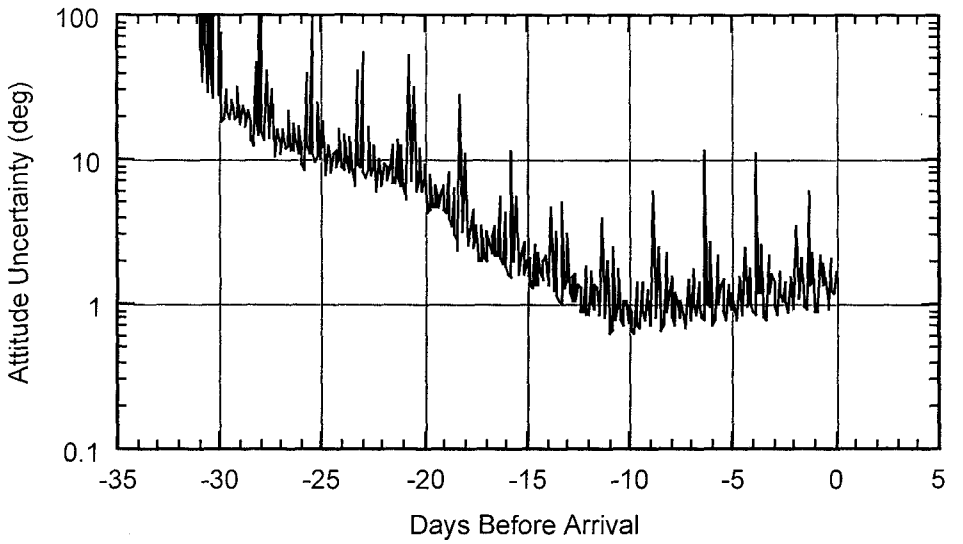

Figure 14 Predicted attitude 1-σ uncertainties after –10 days for Body 2.

To test for the predictability of a complex rotation case, we ran the Body 2 reference case again, but without data after –10 days so that uncertainties were mapped forward in time (i.e., predicted) beyond that point. Figure 14 indicates that orbit designs based on rotation knowledge at –10 days will see body attitude errors averaging under 2 degrees at arrival time. Thus attitude knowledge for all four reference cases seems adequate for orbit design to proceed by the –10 day mark or earlier.

Reference Cases – Trajectory Knowledge

Although it is not critical information for the design of the orbital phase, the uncertainty in the position of the spacecraft is of interest in a general sense. Figure 15 shows the uncertainty in the inertial position of the spacecraft for the four reference cases. As shown, the smaller the body, the better determined is the spacecraft position. This is due to the strength of the optical data because the trajectory is closer, point-by-point at given times, for the smaller bodies than the larger ones, and the same optical angular errors correspond to smaller metric errors. Even though the Doppler data is stronger for the larger bodies, it only acts in one dimension while the optical data improves the solution in two dimensions. The inflection point visible in all four cases, 11 days prior to arrival, coincides with the slow down maneuver.

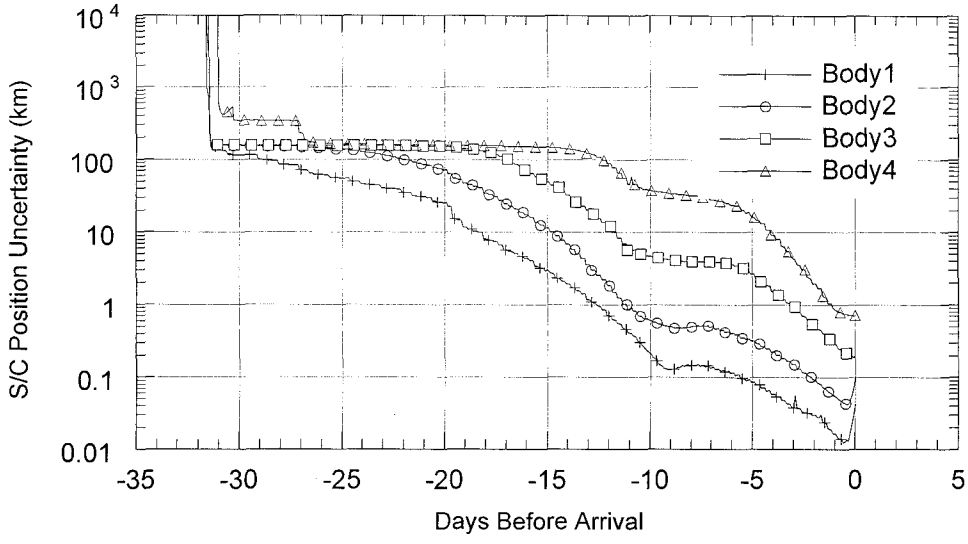

Figure 15 Body centered inertial spacecraft position 1-σ uncertainty (RSS of 3 components) for the four reference cases

Variations – Approach Trajectories

The first parameter to be altered from the reference cases is the geometry of the approach trajectory. Part of the motivation is to see if the GM determination can be improved for the two smaller comets. In the reference cases, the approach occurs from the direction of the Sun and the arrival point is in the terminator plane. For the variations, each of the alternate approach trajectories given in Table 4 is applied to the Body 2 scenario, with all other assumptions unchanged. The GM uncertainties for all six scenarios are plotted in Figure 16 where the trajectory numbers correspond to the numbers given in the plot (Trajectory 1 corresponds to the reference case). The six different trajectories use three different approach directions, resulting in three pairs of trajectories with the same approach directions. Trajectories 1 and 4 approach the body from the Sun-line, trajectories 2 and 5 approach from a 90° solar phase angle, while trajectories 3 and 6 approach from behind the terminator plane, from a 135° solar phase angle. The only difference between each of the paired trajectories is the location of the arrival point.

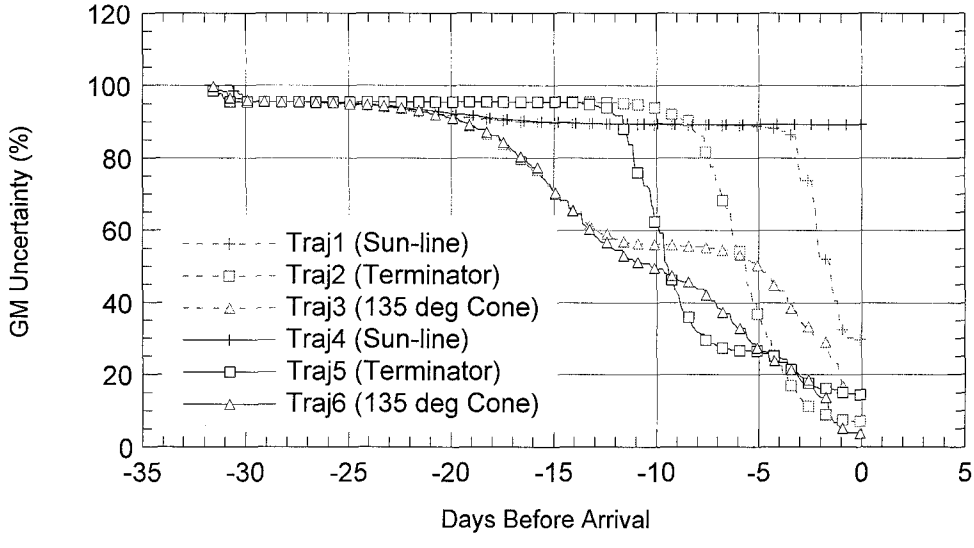

Figure 16 Body 2 scenario: GM 1-σ uncertainty for alternate approach trajectories

The complex results of the GM uncertainty in Figure 16 need some explanation. The early portion of the uncertainty history is similar between each of the three pairs of trajectories with the same approach directions, but there is considerable variation at the end.

Considering the trajectory pair approaching from the sun, the filter is never able to adequately separate the GM from the comet outgassing parameters for trajectory 4, which terminates on the sun-line, and thus the uncertainty never goes below about 90%. This is clearly not desirable. The other trajectory (#1), which is offset from #4 and ends in the terminator plane, allows the filter to rapidly decorrelate outgassing and gravity in the last four days. Reference to Figure 9 makes this easy to understand. However, the results for either of these two trajectories are clearly less desirable than for the other four.

For the trajectory pair in the terminator plane (#2 and #5; actually #5 is parallel to but slightly offset from the terminator plane), a similar effect is seen about 12 days before arrival. The GM knowledge improves more rapidly at first for #5 but at the end #2 achieves the smaller uncertainty. Understanding of this is also aided by reference to Figure 9, where it can be seen that trajectory #5 will benefit in the later part of the approach by "feeling" the comet's gravity along a more favorable direction (nearer the earth-line) for Doppler sensitivity before it enters the region where the gravity is masked by outgassing. Trajectory #2 never enters the heavy outgassing region, and likely achieves its good performance at the end through a combination of the slight but non-zero component of the gravity force along the earth-line and the trajectory bending which optical data begins to sense near the end.

For the trajectory pair approaching from 135° solar phase angle (#3 and #6), the initial mass determination begins earlier because there is better Doppler sensitivity and negligible outgassing. At –13 days, the results separate so that the trajectory ending sunward of the terminator plane yields the best final mass knowledge of all the trajectories, while the one ending at the terminator plane achieves mediocre results. The differing results for these two trajectories are difficult to understand, so we will simply point out a few plausible causes and save a detailed analysis for another time: (1) Trajectory 6 ends at a point of moderate Doppler sensitivity to gravity still away from the heaviest outgassing region, while trajectory 3 ends (at the same arrival radius of ~100 km) at a point of nearly zero Doppler sensitivity. (2) Trajectory 6 passes through the terminator plane where the outgassing incidence angle on the solar panels passes through zero degrees, which may help the filter to decorrelate outgassing and gravity. (3) In the last few days on trajectory 6, more optical landmark data is available since the spacecraft sees more of the sun-illuminated surface.

We summarize GM determination from an orbit planning perspective for this heavy outgassing case: • The sun-line is the worst direction to approach from. • Approaching in the plane of the terminator or from behind it to avoid the worst outgassing yields the best results. • Location of the arrival point can make a significant difference (for which it is difficult to make a generalizing statement), but ... • In all of these approaches, GM is not well determined until very late in the approach. This last observation means that detailed orbit design may have to be done very quickly at the end of the approach, or that the mission may have to allow for stages of orbit design from rough to detailed as GM is better determined in the initial orbit, or that the mission may have to rely on non-ballistic trajectories (essentially ignoring gravity) for the orbit phase, at considerable expense of fuel.

For the rest of the parameters -- the body attitude and the outgassing strength -- results are given in tabular form in Table 12. This table gives the uncertainties for each parameter at 25, 15, 5, and 0 days before arrival for Body 2 with the six different arrival trajectories. The attitude parameters and outgassing strength all are determined best when approaching the body from the Sun direction (as in trajectory #1 and #4), which is opposite the results obtained for GM. Attitude is well determined because the body is always

fully illuminated, and this is determined almost solely on the strength of the optical navigation tracking data. Figure 17 shows that optical data coverage of landmarks is strongly reduced when approaching from high phase angles, which supports the findings in the table. Outgassing is also determined best when approaching from the sun because that is the direction that forces are largest. From Table 12, it does not seem that the arrival point location is critical to the amount of time required to determine body attitude. However, obviously it can be important in determining outgassing strength.

Table 12
IMPACT OF THE APPROACH TRAJECTORY ON THE 1-σ UNCERTAINTIES IN THE BODY 2 PHYSICAL PARAMETERS

	Traj1 (Sun-line)	Traj2 (In Term.)	Traj3 (135 cone)	Traj4 (Sun-line)	Traj5 (In Term.)	Traj6 (135 cone)
Attitude:						
25 days out	11.7°	16.4°	103.1°	12.4°	16.1°	98.4°
15 days out	2.0°	3.0°	16.9°	1.9°	1.6°	3.0°
5 days out	0.5°	0.6°	1.8°	0.3°	0.5°	1.5°
At Arrival	0.3°	0.4°	0.6°	0.1°	0.3°	0.4°
Outgassing Strength:						
25 days out	96.3%	100.0%	100.0%	98.1%	100.0%	100.0%
15 days out	67.5%	100.0%	100.0%	68.8%	100.0%	100.0%
5 days out	65.2%	99.9%	99.9%	65.1%	88.6%	99.0%
At Arrival	58.3%	98.9%	99.6%	64.8%	55.2%	57.7%

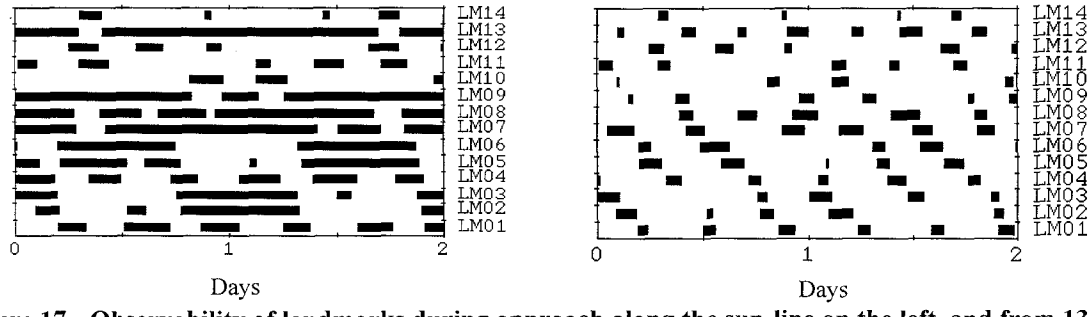

Figure 17 Observability of landmarks during approach along the sun-line on the left, and from 135° solar phase angle on the right, for Bodies 1–3 reference cases (complex rotation). Two days are shown, near the beginning of the trajectory.

Table 13 compares trajectory #1 (the reference cases) to trajectory #2 in terms of GM, attitude, and outgassing strength uncertainties for Bodies 1, 3, and 4. For Body 1, the differences between approaching from the Sun direction and approaching in the terminator plane are very similar to the differences observed for Body 2, i.e., the GM is determined more quickly when the approach is in the terminator plane (trajectory #2), while the other parameters are determined earlier when the approach is from the Sun direction.

Table 13
IMPACT OF THE APPROACH TRAJECTORY ON THE 1-σ UNCERTAINTIES IN THE BODY 1, 3 AND 4 PHYSICAL PARAMETERS

	Body 1		Body 3		Body 4	
	Traj1 (Sun-line)	Traj2 (In Term.)	Traj1 (Sun-line)	Traj2 (In Term.)	Traj1 (Sun-line)	Traj2 (In Term.)
GM:						
25 days out	95.5%	95.5%	49.5%	94.4%	6.9%	77.1%
15 days out	95.4%	95.5%	11.8%	80.5%	0.5%	14.0%
5 days out	95.4%	73.2%	7.6%	2.0%	0.1%	0.2%
At Arrival	84.7%	25.4%	1.4%	0.2%	0.0%	0.0%
Attitude:						
25 days out	11.4°	14.5°	17.9°	13.5°	23.5°	49.3°
15 days out	2.0°	3.7°	3.1°	4.5°	3.1°	5.1°
5 days out	0.4°	0.6°	0.6°	0.8°	0.6°	1.1°
At Arrival	0.3°	0.3°	0.4°	0.4°	0.2°	0.4°
Outgassing Strength:						
25 days out	96.0%	100.0%	99.7%	100.0%	NA	NA
15 days out	61.9%	100.0%	99.6%	100.0%	NA	NA
5 days out	58.5%	87.8%	85.8%	100.0%	NA	NA
At Arrival	57.7%	71.7%	58.5%	99.8%	NA	NA

For Body 3, GM is better determined early-on when the approach is from the Sun, which is opposite the situation for Bodies 1 and 2. This is because the gravitational / outgassing acceleration is much larger (Figures 8–10). Later in the approach trajectory 2 ultimately allows better determination of GM. The remaining parameters follow the same patterns observed for Body 1 and 2, i.e., the body orientation parameters are determined slightly earlier when approaching the body from the Sun line, and the outgassing strength is only determined when approaching from the Sun line.

Body 4 is an asteroid and there is no outgassing. The body attitude knowledge follows the same trend seen for the other bodies, with earlier parameter determination possible when approaching the body from the Sun direction. Without the effects of outgassing, the GM is better determined throughout the entire time span when the approach is made from the Sun direction.

Variations – Comet versus Asteroid

To see exactly how outgassing impacts the determination of the other physical parameters, the Body 2 and 3 reference cases (approach along the sun-line) are repeated without outgassing. These scenarios would approximate a mission to a small to mid-sized asteroid. Results are given in Table 14 along with the reference results. As expected, GM is better determined. The improvement is more drastic for Body 2 compared to Body 3. Nevertheless, there is still significant improvement in GM determination in the later part of the approach for Body 3.

Table 14
IMPACT OF OUTGASSING ON THE 1-σ UNCERTAINTY IN THE BODY 2 AND 3 PHYSICAL PARAMETERS

	Body 2		Body 3	
	Reference	Asteroid	Reference	Asteroid
GM:				
25 days out	94.7%	94.6%	49.5%	48.8%
15 days out	89.6%	46.2%	11.8%	4.8%
5 days out	88.6%	1.5%	7.6%	0.1%
At Arrival	29.8%	0.2%	1.4%	0.0%
Attitude:				
25 days out	11.7°	12.3°	17.9°	17.9°
15 days out	2.0°	2.1°	3.1°	3.1°
5 days out	0.5°	0.5°	0.6°	0.6°
At Arrival	0.3°	0.4°	0.4°	0.4°

Variations – Complex versus Simple Rotation

All of the scenarios examined to this point have assumed that the body is under complex rotation, with the exception of Body 4. To see the impact of this assumption, the Body 2 reference case is rerun using simple rotation and the Body 4 reference case is rerun using complex rotation (Case 3, Table 5). Table 15 summarizes the impact of switching the rotation scheme. Not surprisingly, there is very little difference in GM determination. Attitude is determined slightly earlier when the body is in complex rotation. The likely reason is that the complex rotation allows more of the body to be visible during the approach, yielding better observability of landmarks (Figure 17). As an example, 107 landmark observations are made in the Southern hemisphere during the Body 2 reference case, while there are none in that region when the body is in a simple rotation.

Table 15
IMPACT OF COMPLEX VERSUS SIMPLE ROTATION ON THE 1-σ UNCERTAINTY IN THE BODY 2 AND 4 PHYSICAL PARAMETERS

	Body 2		Body 4	
	Reference	Simple	Reference	Complex
GM:				
25 days out	94.7%	96.4%	6.9%	7.2%
15 days out	89.6%	91.0%	0.5%	0.5%
5 days out	88.6%	89.9%	0.1%	0.1%
At Arrival	29.8%	28.8%	0.0%	0.0%
Attitude:				
25 days out	11.7°	16.3°	28.7°	27.7°
15 days out	2.0°	2.8°	3.1°	2.2°
5 days out	0.5°	0.5°	0.6°	0.4°
At Arrival	0.3°	0.2°	0.2°	0.1°

Variations – Angular Momentum Direction

Each of the directions for the angular momentum pole, as outlined in Table 6, were used in the Body 2 scenario. There was very little difference between the time required to determine the uncertainty in the GM, the body attitude, and the outgassing strength. However, some slight differences are apparent in spin rate uncertainties. The spin rate uncertainty for cases 2 and 3 (Table 6) were virtually identical, meaning that the clock angle of the rotation angular momentum vector is not an important factor in this respect. Figure 18 shows the spin rate uncertainty time history for the two extreme cases, #1 and #4 in Table 6, where the rotation angular momentum vector is pointed either towards either the Sun or 90° from the Sun. The two intermediate cases (#2 and #3) fall between these two extremes. The instantaneous rotation rate is determined a little more accurately during the approach when the rotation angular momentum vector is pointed 90° from the Sun, but this distinction is probably trivial.

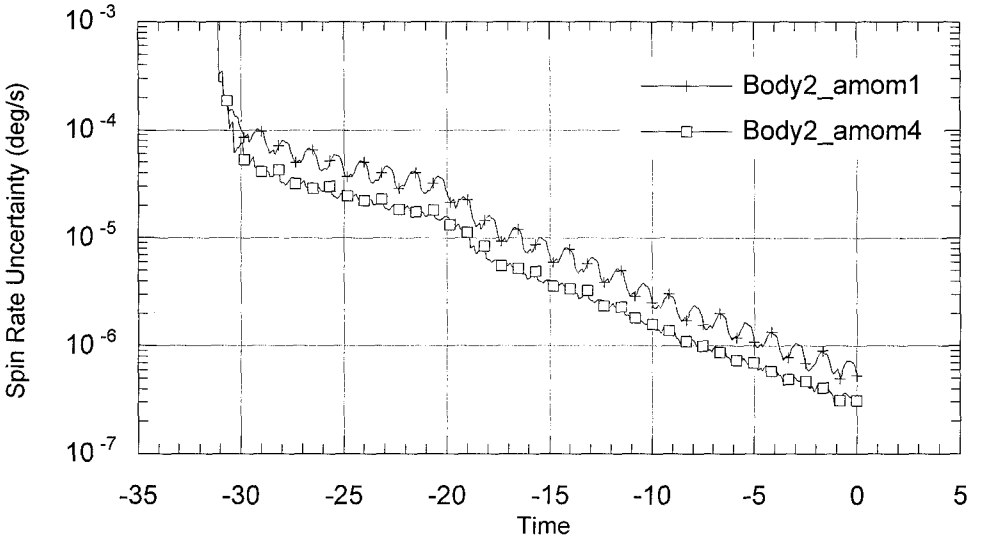

Figure 18 Body 2 scenario: Spin rate 1-σ uncertainties for different rotation angular momentum orientations

Variations – Tracking Data Rates

This section indicates the effect of tracking data frequency on parameter determination, as shown in Table 16. The comparisons also show the relative strengths of the radiometric and optical navigation tracking data. The Body 2 reference case is run with each of the tracking data schedules defined in Table 8.

Comparing the high rate case with the reference case, the more frequent observations do not improve the uncertainty in GM until very late in the approach. However, the uncertainty in the position of the spacecraft does show improvement throughout the entire time frame. The increased frequency of the opnav data slightly helps the early estimates of the body attitude, but does not provide much added certainty to these parameters later in the approach. The uncertainty in the outgassing strength is virtually the same between the high, medium, and low data rate frequencies. Further examination of the low-rate frequencies shows that the GM is determined at approximately the same level of certainty until the end of the approach, where it is slightly less well determined in comparison with the reference case. The estimates of the spacecraft position show further degradation with the low data rate, compared with the reference case. Also, the uncertainty in the body attitude increases significantly when going from the reference case to the low data rate case, especially early in the approach phase.

In summary, increasing the data rates seems to have a small effect on the determination of GM

until late in the approach phase. The uncertainty in the spacecraft position is the most sensitive to the data rate used. Additionally, the body orientation parameters are determined better early in the approach when the higher data rates are used, although the differences later in the approach are minimal. However, the choice between the three data rates tested seems to have a very small impact on the uncertainty of the outgassing strength.

Table 16
IMPACT OF DATA SCEHDULE ON THE BODY 2 PHYSICAL PARAMETERS

	High Rate (Case #1)	Moderate (reference)	Low Rate (Case #3)	Radio (Case #4)	Optical (Case #5)
GM:					
25 days out	94.7%	94.7%	94.8%	100.0%	95.5%
15 days out	89.6%	89.6%	89.6%	96.7%	95.5%
5 days out	88.6%	88.6%	88.7%	92.1%	91.2%
At Arrival	10.0%	29.8%	32.9%	73.4%	33.4%
Position:					
25 days out	127.3 km	141.2 km	152.2 km	335.7 km	405.6 km
15 days out	8.0 km	11.3 km	16.4 km	333.9 km	28.9 km
5 days out	0.2 km	0.3 km	0.5 km	335.9 km	1.5 km
At Arrival	0.03 km	0.10 km	0.14 km	228.5 km	4.8 km
Attitude:					
25 days out	8.2°	11.7°	24.8°	NA	12.4°
15 days out	1.4°	2.0°	5.0°	NA	1.9°
5 days out	0.4°	0.4°	1.0°	NA	0.3°
At Arrival	0.2°	0.2°	0.6°	NA	0.1°
Outgassing Strength:					
25 days out	96.3%	96.3%	96.7%	99.9%	100.0%
15 days out	67.5%	67.5%	67.5%	85.2%	100.0%
5 days out	65.1%	65.2%	65.2%	65.8%	78.3%
At Arrival	57.3%	58.3%	58.6%	63.3%	59.9%

The radiometric only scenario (Case 4) shows significantly higher uncertainties in both the GM and spacecraft position estimates. Not surprisingly, the radiometric data alone can not provide significant information on the attitude of the body during the approach. The higher uncertainty in the outgassing strength for the radiometric only case is not as drastic as for the other parameters. The opnav only scenario (Case 5) is interesting to compare to the radiometric only case. Both the GM and the spacecraft position are determined better by the opnav data than by the radiometric data, although the uncertainty in the spacecraft position is still quite large at arrival. The attitude of the body is determined almost as well in the opnav only case as the reference case. However, the outgassing is determined better by the radiometric data than the opnav data. This shows that the combination of the two types of data supplement each other well in determining the parameters required during approach to a small body in order to allow the design of the orbital phase of a small body mission.

APPROACH TIMELINE AND SOME POST-ARRIVAL CONSIDERATIONS

Table 17 shows a hypothetical timeline for approaching Body 2. Trajectory 2 is flown (approach in the terminator plane) for its better mass determination characteristics. Even so, the mass is determined so late that the final orbit design cannot be completed before arrival and a suboptimal orbit is entered for an undetermined number of days until the mass estimate is good enough for a final design.

Table 17
HYPOTHETICAL TIMELINE FOR APPROACH TO BODY 2 IN TERMINATOR PLANE

Time (days)	Activity/Condition	Navigation Products (1-σ)
–32	1. Arrive 10000 km from Body 2 in terminator plane 2. Slow to ~5 m/s & target to nominal arrival point 3. Image diameter = 35 pixels 4. Designate and track landmarks to get rough pole and rotation 5. Begin search for co-orbitals or large debris	1. 200 km s/c ephemeris
–25	0. 7500 km, 47 pixels. 1. Retarget to new arrival point based on crude rotation ephemeris and pole direction.	1. Initial estimate of pole direction 2. Crude rotation ephemeris (~15 deg)
–16	0. 4000 km, 88 pixels 1. Refine pole and rotation estimates 2. Crude topography model 3. Mass estimate from topography model & assumed density 4. Generate crude orbit design using estimated rotation ephemeris & mass	0. Rotation ephemeris (~4 deg) 1. 20 km s/c ephemeris 2. Mass estimate ~90% of nominal 3. Initial body-fixed coordinate system
–11	0. 1000 km, 352 pixels 1. Refine targeting 2. Slow to ~1m/s 3. Update topography model & re-estimate mass	0. Rotation ephemeris (~2 deg) 1. Adjusted mass estimate, 90% 2. 1 km s/c ephemeris
-5	• 400 km, 880 pixels • Update orbit design based on revised mass • Retarget based on revised mass	0. Mass estimate, ~40% 1. 500 m s/c ephemeris 2. Rotation ephemeris (~0.5 deg) 3. Final body-fixed coordinate system
0	• Arrival at 100 km in terminator plane • Enter initial orbit • Update orbit design • Continue refining mass estimate	• Mass estimate ~ 10% • 100 m s/c estimate • Initial outgassing estimate
+n	Generate final orbit design	• Final mass estimate • Final outgassing estimate

Projects with ample fuel margins which can afford to ignore gravity and drive around in non-ballistic orbits with time at a premium may not need an early determination of mass. For other projects with restricted fuel budgets but ample time for ballistic trajectories, mass determination is more important. As an example of these extremes, Figure 19 shows sample orbit phases for the now defunct Champollion mission which would have landed on Tempel 1, and the not-yet-approved CNSR (Comet Nucleus Sample Return) mission. For all the time (three months) and complexity of the Champollion orbit phase, the deterministic fuel cost was only about 3 m/s (Ref 14). Conversely, the cost for CNSR's 27 days in orbit is about 14 m/s (Ref 15), and would have been more fuel-expensive for shorter times.

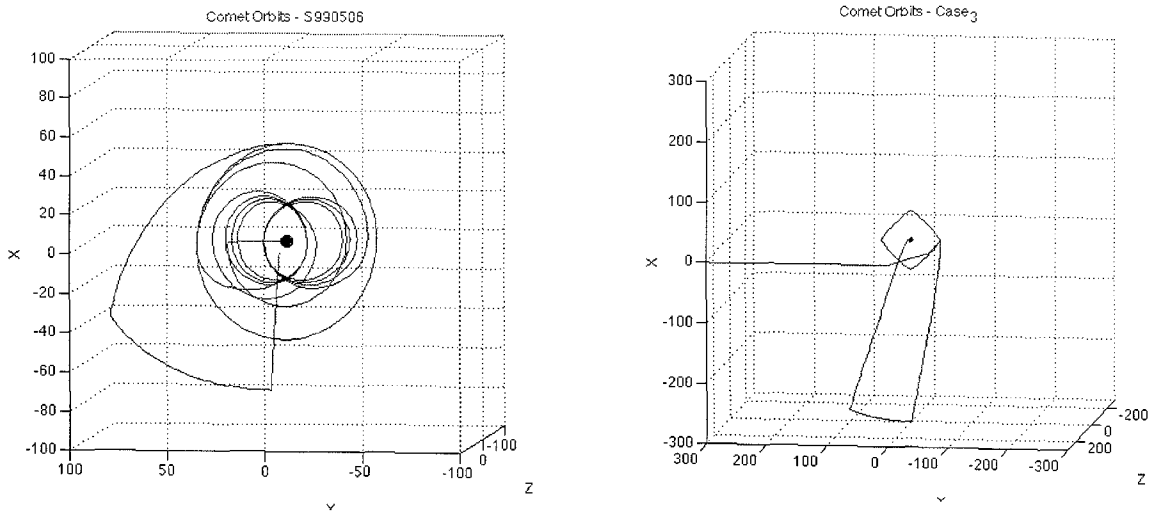

Figure 19 The complex orbit phase of the Champollion mission on the left would have required about three months to complete, involving a global mapping phase from about 50 km radius followed by multiple 13 km flyovers of potential landing sites, mapping the sites to the 1 meter level before one was chosen for landing. The simple, non-ballistic orbit phase of CNSR on the right was motivated by the desire to spend as little time as possible in orbit in a hazardous dust environment before landing. Time for the orbit shown, from arrival to landing, was about 27 days.

CONCLUSIONS

We have done a sparse sampling of the scenario space outlined at the outset of this paper. We evaluated scenarios for four different body sizes, three different approach directions, and several other conditions including variations of outgassing, rotation, arrival points, and tracking data. Subject to the assumptions we have listed, we come to the following conclusions:

1. For most scenarios, rotation characteristics are determined well enough and early enough for mission decisions based on modeling and prediction of body attitude to within a few degrees of error (e.g., less than 5°) to be made before arrival (e.g., 15 days).
2. For small to moderate sized comets (radii on the order of 0.5 to 3 km) with strong outgassing, approach from the sunward direction yields poor determination of mass, which will make it difficult to accomplish detailed ballistic orbit design before arrival. Approach in the plane of the body terminator or from behind it may allow sufficient determination of mass for orbit design to proceed before arrival, but probably by not more than a few days (e.g., 5).
3. Comet outgassing strength for any size comet is never well determined on approach (never better than 50% of nominal in our scenarios), and orbit design should take this into account for small comets with strong outgassing (e.g., by orbiting near the terminator plane).
4. For very large comets with radii on the order of 25 km (e.g., Hale-Bopp), early mass determination is achievable even with strong outgassing and even on approach from the sun direction (although missions would likely have other reasons for avoiding that direction).
5. For small to large asteroids (radii on the order of 3 to 250 km), the best approach direction for early mass determination is along the earth-line (which is near the sun-line in our scenarios) where Doppler sensitivity is greatest . Mass is determined early enough in the approach to the larger bodies that detailed orbit design could proceed at 15 days before arrival or earlier. For the smallest asteroid (3 km), design would probably have to wait until sometime between 5 and 15 days before arrival.

Design of the orbit phase of missions to previously unvisited small bodies will depend largely on

information gathered in the last weeks or days of the approach. We hope that this paper will be useful as a guideline for selecting approaches that are efficient in determining parameters necessary to orbit design, and for avoiding approaches counterproductive to that end.

ACKNOWLEDGEMENTS

In the course of this analysis, it was necessary to upgrade portions of the JPL standard navigation software set to handle aspects of the modeling. We are indebted to the following people without whose efforts the analysis could not have been done: J.K. Miller, who provided the formulation used for integrating attitude and attitude partials for a generally rotating body, and M. Sengstacke, who implemented those formulations; D.J. Scheeres, who provided the spherical harmonic formulation for comet outgassing and useful information on rotation characteristics; R.F. Sunseri, who integrated the rotation and outgassing models into the JPL Orbit Determination Program, and W.M. Owen, Jr., who implemented them in the optical navigation software suite, along with a capability to use the small body ephemeris file.

The authors also thank F.M. Stienon for useful discussions on (and a formulation for) mapping rotation covariances, J.K. Miller for his suggestion for the generic ratios we used for small body axes, and M.M. Watkins for providing a managerial boost at a crucial time.

The research described in this paper was performed at the Jet Propulsion Laboratory, California Institute of Technology, under contract with the National Aeronautics and Space Administration.

REFERENCES

1. Enzian, A., Weissman, P.R., Gaskell, R.W., Goodwin, D.G., Scheeres, D.J., Bhargava, S., "Periodic Comets 46P/Wirtanen and 9P/Tempel 1: Gas Dynamical Modeling of the Near-Nucleus Coma Environment", poster 14.17-P presented at the Asteroids, Comet, Meteors 2000 meeting at Cornell University, July 2000.

2. Gill, E., Montenbruck, O., and Patzold, M., "Perturbation Forces Acting on the Rosetta Spacecraft in a Close Orbit Around Comet P/Wirtanen", Paper AAS 96-150, AAS/AIAA Space Flight Mechanics Meeting, Austin, Texas, 12-15 February 1996.

3. Helfrich, C.E., Miller, J.K., Antresian, P.G., Carranza, E., and Williams, B.G., Near Earth Asteroid Rendezvous (NEAR) Revised Orbit Phase Trajectory Design", Paper AAS 99-464, AAS/AIAA Astrodynamics Specialist Conference, Girdwood, Alaska, 16–19 August 1999.

4. Miller, J.K., Williams, B.G., Bollman, W.E., Davis, R.P., Helfrich, C.E., Scheeres, D.J., Synnott, S.P., Wang, T.C., and Yeomans, D.K., "Navigation Analysis for Eros Rendezvous and Orbital Phases", The Journal of the Astronautical Sciences, Vol. 43, No. 4, October–December 1995, pp. 453–476.

5. Miller, J.K., Weeks, C.J., and Wood, L.J., "Orbit Determination of the Comet Rendezvous/Asteroid Flyby Mission: Post-Rendezvous Phases", Paper AIAA-89-0348, AIAA 27th Aerospace Sciences Meeting, Reno, Nevada, 9–12 January 1989.

6. Owen, W.M., personal commication, Jet Propulsion Laboratory, October 2000.

7. Scheeres, D.J., "Analytic Descriptions of Small-Body Rotational Motion", Final Report of California Institute of Technology contract 1211309 with the University of Michigan for the Comet Force Environment Simulation Project, 25 August 2000.

8. Scheeres, D.J., Bhargava, S., and Enzian, A., "A Navigation Model of the Continuous Outgassing Field Around a Comet", JPL TMO Progress Report 42-142, 15 August 2000.

9. Scheeres, D.J., Marzari, F., Tomasella, L., and Vanzani, V., "ROSETTA mission: satellite orbits around a cometary nucleus", Planet. Space Sci., Vol. 46, No. 6/7, pp. 649–671, 1998.

10. Scheeres, D.J., Ostro, S.J., Hudson, R.S., DeJong, E.M., and Suzuki, S., "Dynamics of Orbits Close to Asteroid 4179 Toutatis", Article No. IS975870, Icarus 132, 53–79, 1998.

11. Scheeres, D.J., Williams, B.G., and Miller, J. K., "Evaluation of the Dynamic Environment of an Asteroid: Applications to 433 Eros", Paper AAS 99-158, AAS/AIAA Space Flight Mechanics Meeting, Breckenridge, Colorado, 7–10 February 1999.

12. Scheeres, D.J., Williams, B.G., Bollman, W.E., Davis, R.P., Helfrich, C.E., Synnott, S.P., and Yeomans, D.K., "Navigation for Low-Cost Missions to Small Solar-system Bodies", IAA-L-0302P, IAA International Conference on Low-Cost Planetary Missions, 12–15 April 1994.

13. Standish, E.M., "JPL Planetary and Lunar Ephemerides, DE405/LE405", JPL Interoffice Memorandum 312.F -98–048 (internal document), Jet Propulsion Laboratory, Pasadena, California, 26 August 1998.

14. Taylor, A.H. and Bordi, J.J., "CNSR Strawman Approach/Orbit Scenarios", Presentation to JPL CNSR Mission Design Team (internal document), Jet Propulsion Laboratory, Pasadena, California, 19 May 2000.

15. Taylor, A.H., "ST4 Near-comet Mission Scenario, Case: S990506", Presentation to JPL ST4 Mission Design Team (internal document), Jet Propulsion Laboratory, Pasadena, California, 5 May 1999.

16. Yeomans, D.K., et. al., "Comet 9P/Tempel 1 orbit, ephemeris, and uncertainty analysis", JPL Interoffice Memorandum 312.F -99–069 (internal document), Jet Propulsion Laboratory, Pasadena, California, 5 May 1999.

APPENDIX

Outgassing coefficients

The α_{ij} and β_{ij} used to define the shape of the outgassing field used in this analysis are given in Table A1.

Table A1
OUTGASSING COEFFICIENTS

i \ j	0	1	2	3	4
			α_{ij}		
1	1.7424380e0	2.4954340e-1			
2	8.0649220e-1	1.0767340e-1	1.2179830e-2		
3	-1.6492650e-2	-4.0825580e-3	-1.5942440e-3	-3.3663670e-4	
4	-6.4582310e-2	-9.6370230e-4	-2.0065580e-3	-9.4770940e-5	-1.2518440e-4
			β_{ij}		
1	0	-3.2874030e-3			
2	0	-1.7287340e-3	4.2847190e-4		
3	0	3.1134650e-3	-7.3604510e-4	-1.3549240e-4	
4	0	4.2770650e-3	-5.6703060e-4	-9.6860660e-5	2.1226330e-5